PAPER

SWIR emissive RosIndolizine dyes with nanoencapsulation in water soluble dendrimers†

Satadru Chatterjee, [a] William E. Meador, [a] Cameron Smith, [a] Indika Chandrasiri, [a] Mohammad Farid Zia, [b] Jay Nguyen, [b] Austin Dorris, [a] Alex Flynt, [b] Davita L. Watkins, [a] Nathan I. Hammer [a] and Jared H. Delcamp *[a]

Shortwave infrared (SWIR) emission has great potential for deep-tissue *in vivo* biological imaging with high resolution. In this article, the synthesis and characterization of two new xanthene-based RosIndolizine dyes coded [Ph]RosIndz and [tol]RosIndz is presented. The dyes are characterized *via* femtosecond transient absorption spectroscopy as well as steady-state absorption and emission spectroscopies. The emission of these dyes is shown in the SWIR region with peak emission at 1097 nm. [Tol]RosIndz was encapsulated with an amphiphilic linear dendritic block co-polymer (LDBC) coded 10-PhPCL-G3 with high uptake yield. Further, cellular toxicity was examined *in vitro* using HEK (human embryonic kidney) cells where a >90% cell viability was observed at practical concentrations of the encapsulated dye which indicates low toxicity and reasonable biocompatibility.

1 Introduction

Fluorescence biological imaging in the shortwave (SWIR or NIR-II) infrared spectral region from 1000 nm to 2000 nm is a powerful technique for high definition real-time non-invasive monitoring of biological systems.[1–7] Importantly, small molecule fluorescent probes have made a profound impact in chemical biology, clinical diagnosis, and photo-theranostics.[6,8–13] However, relatively few probes exist in the SWIR region, which allows for the deepest tissue penetration since background noise due to tissue autofluorescence and biological matrix absorption are minimal.[14,15] The lack of SWIR probes limits fluorescence imaging application progress in terms of imaging depth and with regard to multiplex imaging probe options. Many of the reported probes in the SWIR region are based on carbon nanotubes or quantum dots which suffer from indefinite distribution in organs or from slow excretion kinetics.[16,17] Small molecule based organic dyes for SWIR imaging are attractive materials that often offer good biocompatibility relative to many inorganic materials.[3,18–24]

Xanthene-based dyes are popular fluorophore probes in the visible region due to their excellent molecular brightness (MB), biocompatibility, and photostability.[25–28] MB is defined according to the equation $MB = \varepsilon \times \phi$, where ε is the molar absorptivity and ϕ is the quantum yield which is the number of photons emitted divided by the number of photons absorbed. Commonly, the materials utilizing xanthene cores rely on amine (rosamines) or oxygen/nitrogen (rosol) mixed donor groups to delocalize the positive charge throughout the π-system. These systems typically fall short of the SWIR spectral region for absorption and emit primarily at higher energy than the SWIR region (for example materials see Fig. 1).[29,30] The use of a carbon substitution such as with an indolizine heterocycle on the xanthene core allows for extension of the π-conjugated system onto the donor group beyond the atom attached to the xanthene core.

Indolizine donors uniquely have a planar geometry and are proaromatic with a pyridinium generated upon electron donation.[31] This is similar to thiopyran and pyran donors which generate aromatic thiopyrylium and pyrylium groups *via* formal valence bond theory drawings. Interestingly, indolizine is also aromatic in the ground state which imparts added stability but still provides electron donation strengths similar to amine groups. The strong donation of indolizine allows for the
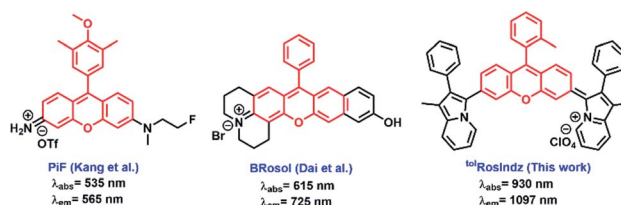
[a]Department of Chemistry and Biochemistry, University of Mississippi, Coulter Hall, University, MS 38677, USA. E-mail: delcamp@olemiss.edu

[b]Department of Biological Sciences, University of Southern Mississippi, Hattiesburg, MS 39406, USA

Fig. 1 Recently reported rosamine and rosol dyes along with RosIndz presented in this work.

retention of cyanine band structuring when indolizine is used in pentamethine and squaraine core systems.[32–34] Recent work from our group has shown that the substitution of amines for indolizine on rhodamine led to a dramatic red-shift of the absorption and emission spectrum with SWIR emission observed.[35] However, the synthesis of the rhodindolizine was challenging and obtaining pure material from the harsh conditions required to open the lactone ring was problematic. This work puts forward a readily accessible rosindolizine dye (RosIndz) that is obtainable on a significant scale with high purity through simple purification procedures. RosIndz has an absorption curve tail extending into the SWIR region and an emission maximum in the SWIR region which is promising for biological imaging applications. Additionally, successful nano-encapsulation in a water-soluble nanoparticle is demonstrated with weak emissive properties being retained.

2   Results and discussion

RosIndz is readily synthesized from known bisborylated compound **1** (ref. 36) in three steps with 49% overall yield (Scheme 1). The synthesis begins with a bromination of compound **1** with stoichiometric $CuBr_2$ to give dibromo inter-mediate **2**. A palladium catalysed double C–H activation reac-tion with **2** and two indolizine heterocycles (**3**)[31] results in the formation of the bisindolizine xanthone intermediate **4** in 92% after optimization of reaction conditions with respect to cata-lysts, ligand, base, solvent, time, and temperature (see Table S1†). Finally, treatment of compound **4** with o-tolyl magnesium bromide or phenyl magnesium bromide followed by workup with a 2 M $HClO_4$ aqueous solution yielded the desired RosIndz dyes as dark green solids in 63–60% yield.

The final dye forms during the acid workup of the oxyanion intermediate (Scheme S1†). Various acids were tried for the workup; however, aqueous $HClO_4$ provided the dye in high yield and cleanly in the crude reaction. Anhydrous acids and anhy-drides such as TfOH, TFA and triflic anhydride readily convert the oxyanion intermediate to the desired RosIndz compound, but lead to rapid decomposition on the order of seconds to minutes. These approaches were only successful if the exact number of equivalents needed could be titrated into the reac-tion mixture to quench the oxyanion with no excess reagent added. The addition of excess 2 M $HClO_4$ solution readily

formed the dye on large scale without decomposing even when the dye is stored in the mixture overnight. Weaker acids failed to convert the oxyanion into the final oxygen eliminated dye and instead gave the alcohol. The dye could be obtained on a 0.3 gram scale without the use of chromatography through simple precipitation protocols used for the final step.

Concerning aryl group nucleophiles, the stability of the final dye requires the presence of a phenyl group. A range of aliphatic groups of different sizes and a thiophene heterocycle on the dye were found to decompose at varying rates which made isolation of pure material challenging in our hands (Table S2†). Attempts to install larger aryl groups such as 2,4,6-triisopropylbenzene or 2,6-dimethylbenzene as the R group on RosIndz failed to give the oxyanion intermediate (Table S2†).

Photophysical studies were undertaken via absorption and emission spectroscopy. Compounds ^{tol}RosIndz and ^{Ph}RosIndz have similar absorption profiles in toluene with $\lambda_{max}^{abs} = 930$ nm for both compounds (Fig. 2 and Table 1). The absorption onset for both compounds is well within the SWIR region reaching ~1100 nm. Molar absorptivities of 79 500 M^{-1} cm^{-1} and 73 500 M^{-1} cm^{-1} were observed for ^{tol}RosIndz and ^{Ph}RosIndz, respectively. Both absorption curve profiles show vibronic bands characteristic of cyanine dyes with shoulders on the high energy side of λ_{max}^{abs}. ^{tol}RosIndz and ^{Ph}RosIndz were both found to emit in the SWIR region ($\lambda_{max}^{em} = 1097$ nm) with similar emission curve shapes and energies (Fig. 2). The emission onsets of both the dyes were found to be at >1400 nm. The compounds have Stokes shifts of 162 nm (0.20 eV). Notably, the Stokes shifts for both the dyes are large enough that the emis-sion maxima has minimal overlap with the absorption curve which enables imaging near this wavelength with maximal MB and minimal re-adsorption of emitted photons. Quantum yields were also calculated for these dyes and found to be 0.05% and 0.04% for ^{tol}RosIndz and ^{Ph}RosIndz respectively. Excited-state lifetimes (τ) were probed with femtosecond transient
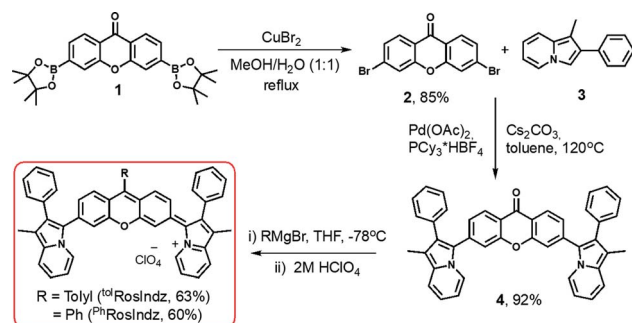
Scheme 1   Synthetic route to prepare the RosIndz dyes.
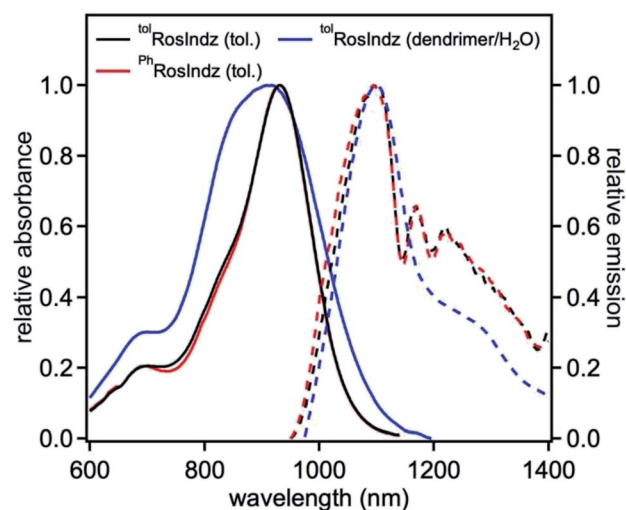

Fig. 2   Normalized absorbance (solid lines) and emission (dashed lines) of dyes in toluene (25 μM, $\lambda_{ex} = 930$ nm) and when nanoencapsulated in water.

Table 1 Photophysical characterization of ^{tol}RosIndz and ^{Ph}RosIndz^a

dye	λ_{max}^{abs} (nm)	λ_{max}^{em} (nm)	ε (M^{-1} cm^{-1})	SS (nm|eV)	ϕ (%)	τ (ps)
^{tol}RosIndz	930	1097	79 500	162|0.20	0.05	—
^{Ph}RosIndz	930	1097	73 500	162|0.20	0.04	—
^{tol}RosIndz^b	918	1099	—	181|0.22	0.01	3.5

^{a} All values are reported in toluene solvent (25 µM) unless otherwise noted. ^{b} Nanoencapsulated *via* amphiphilic polymers (10-PhPCL-G3) and measured in water.

absorption spectroscopy (fsTAS) for the ^{tol}RosIndz dye. Conveniently, a signal in the high energy region could be identified with decay kinetics of 3.5 ps that allows for the monitoring of excited state kinetics (Fig. 3 and S13†). Rapid excited state decay kinetics such as these are typical in the SWIR region.

Density functional theory (DFT) calculations on ^{tol}RosIndz at the B3LYP/6-311G(d,p)[37–39] level of theory with a dichloromethane polarizable continuum model shows the highest occupied molecular orbital (HOMO) and lowest unoccupied molecular orbital (LUMO) delocalized across the entire molecule including the indolizine π-bonds (Fig. 4). The frontier molecular orbital positioning reveals that the π-extended approach with indolizine on xanthene allows for the retention of a low energy π–π* transition involving a mixing of the indolizine and xanthene π-systems with both the HOMO and LUMO. Time dependent (TD)-DFT analysis reveals a single low energy transition separated by 0.34 eV from the next lowest energy transition (Table S4 and Fig. S14†). This large separation suggests the shoulder at 700 nm in the absorption spectrum is vibronic in nature since TD-DFT does not predict any vertical transitions near the lowest energy vertical transition.

Stability studies were conducted under ambient lighting and in the dark under a variety of conditions with ^{tol}RosIndz and ^{Ph}RosIndz (Fig. S9 and S10†). In anhydrous DCM or MeCN, no decomposition is apparent over a 5 hour time period with ^{tol}RosIndz. Very minor loss of absorbance (~2%) is observed under these conditions with ^{Ph}RosIndz. In the presence of acetic acid and water, both dyes decompose to a presumably hydroxylated intermediate which could be exposed to HClO$_4$ to reform the RosIndz dye. The half-life of dye consumption was 3

hours for ^{tol}RosIndz and ~40 minutes for ^{Ph}RosIndz in 1% acetic acid comparing to more than 7 hours and 6 hours in 1% neutral water. The longer stability of ^{tol}RosIndz is attributed to the methyl group sterically blocking one π-face of the dye from nucleophilic attack. In the presence of stronger acids, such as TFA and HClO$_4$, the dyes show no signs of decomposition on the day time scale. Additionally, the dye could be nano-encapsulated (~84 nm particle size) into an amphiphilic linear dendritic block co-polymer (LDBC) coded 10-PhPCL-G3 with high uptake yield compared to a reference material (Fig. S15–S17 and Table S5†).[40] This gives a material stable on the day time scale which is water soluble. Notably, the quantum yield of this material is diminished (0.01%), but emission remains detectable from ~950 nm to >1400 nm (Fig. 2 and S11†).

To test the suitability of the ^{tol}RosIndz dye for bioimaging, toxicity was assessed in the HEK (human embryonic kidney) cell line (Fig. 5 and S18,† purchased from ATCC as 293 [HEK-293]). Dyes loaded into LDBC nanoparticles were added to culture media followed by incubation for 24 hours. Toxicity was quantified using an LDH assay, which reveals that at most
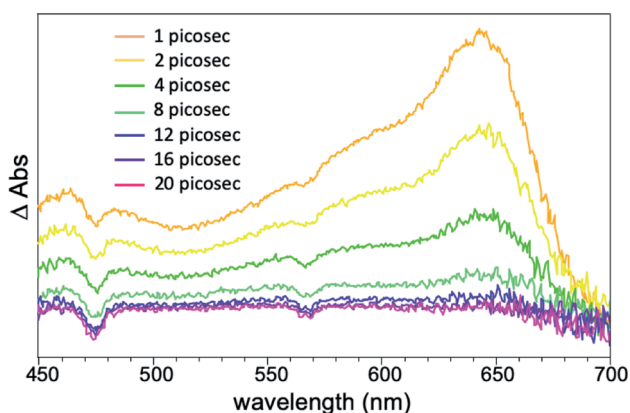
Fig. 3 fsTAS spectral map of encapsulated ^{tol}RosIndz.
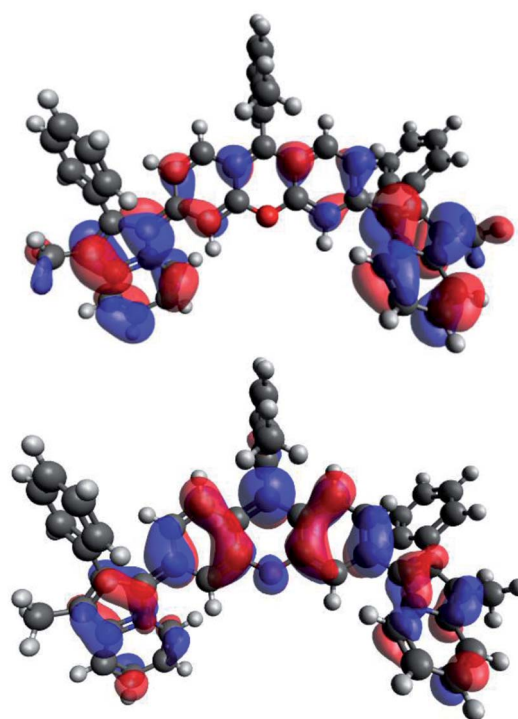
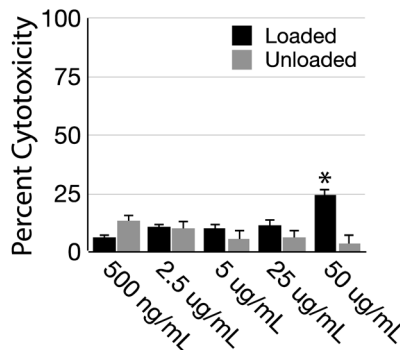**Fig. 4** HOMO (top) and LUMO (bottom) orbitals of ^{tol}RosIndz.

Fig. 5 Toxicity of ^{tol}RolsIndz dye-loaded and unloaded polymer nanoparticles determined by LDH colorimetric assay. Significance difference denoted by "*" was determined by TukeyHSD with a $p \leq 0.5$ threshold.

concentrations any toxicity associated with ^{tol}RosIndz was statistically indistinguishable from unloaded nanoparticles. The exception was the highest concentration (50 µg mL^{-1}) where elevated toxicity was observed. Loss of particle integrity and the subsequent unloading of dye likely leads to elevated toxicity with dye loaded particles since a significant difference is observed between the loaded and unloaded nanoparticles at 50 µg mL^{-1}. Importantly, 1–10 µg mL^{-1} is a typical range used for imaging in our experience where >90% cell viability is demonstrated. Even lower concentrations would work for many dyes in confocal microscopy. Thus, the dye-loaded nanoparticles demonstrate a low toxicity under practical concentrations.

3 Conclusions

In summary, two xanthene-based dyes with indolizine donors in place of oxygen or nitrogen donors have been synthesized and photophysically characterized *via* steady state absorption, steady-state emission, and time-resolved absorption spectroscopies. Both dyes were found to absorb and emit in the SWIR region. Nanoencapsulation of the dye allowed for emission in water which enables biological imaging applications. At the concentrations used in toxicity assays, which are several fold higher than would be used for *in vivo* bioimaging, minimal cell toxicity is observed. This approach presents a novel dye architecture that enables the rational design of small molecule based SWIR probes for deep tissue penetration and high resolution imaging which are in high demand. Efforts to molecularly engineer probes with deeper SWIR emission are underway.

Conflicts of interest

Some of the authors are inventors on a patent application related to these dyes.

Acknowledgements

Notes and references

1 A. L. Antaris, H. Chen, K. Cheng, Y. Sun, G. Hong, C. Qu, S. Diao, Z. Deng, X. Hu, B. Zhang, X. Zhang, O. K. Yaghi, Z. R. Alamparambil, X. Hong, Z. Cheng and H. Dai, *Nat. Mater.*, 2016, **15**, 235–242.

2 J. Cao, B. Zhu, K. Zheng, S. He, L. Meng, J. Song and H. Yang, *Front. Bioeng. Biotechnol.*, 2019, **7**, 487.

3 F. Ding, Y. Zhan, X. Lu and Y. Sun, *Chem. Sci.*, 2018, **9**, 4370–4380.

4 J. Zhao, D. Zhong and S. Zhou, *J. Mater. Chem. B*, 2018, **6**, 349–365.

5 C. Tian and K. Burgess, *ChemPhotoChem*, 2021, DOI: 10.1002/cptc.202000287.

6 H. Dai, Q. Shen, J. Shao, W. Wang, F. Gao and X. Dong, *The Innovation*, 2021, **2**, 100082.

7 Q. Shen, S. Wang, N.-D. Yang, C. Zhang, Q. Wu and C. Yu, *J. Lumin.*, 2020, **225**, 117338.

8 Z. Yang, A. Sharma, J. Qi, X. Peng, D. Y. Lee, R. Hu, D. Lin, J. Qu and J. S. Kim, *Chem. Soc. Rev.*, 2016, **45**, 4651–4667.

9 R. Wang, X. Li and J. Yoon, *ACS Appl. Mater. Interfaces*, 2021, **13**, 19543–19571.

10 S. M. Usama and K. Burgess, *Acc. Chem. Res.*, 2021, **54**, 2121–2131.

11 K. Ilina, W. MacCuaig, M. Laramie, J. N. Jeouty, L. R. McNally and M. Henary, *Bioconjug. Chem.*, 2020, **31**, 194–213.

12 S. Zhu, R. Tian, A. L. Antaris, X. Chen and H. Dai, *Adv. Mater.*, 2019, **31**, 1900321.

13 Q. Wang, Y. Dai, J. Xu, J. Cai, X. Niu, L. Zhang, R. Chen, Q. Shen, W. Huang and Q. Fan, *Adv. Funct. Mater.*, 2019, **29**, 1901480.

14 L. Li, X. Dong, J. Li and J. Wei, *Dyes Pigm.*, 2020, 108756, DOI: 10.1016/j.dyepig.2020.108756.

15 T. Jin, *ECS J. Solid State Sci. Technol.*, 2019, **8**, R9–R13.

16 Z. Liu, C. Davis, W. Cai, L. He, X. Chen and H. Dai, *Proc. Natl. Acad. Sci. U. S. A.*, 2008, **105**, 1410–1415.

17 Y. Zhang, Y. Zhang, G. Hong, W. He, K. Zhou, K. Yang, F. Li, G. Chen, Z. Liu, H. Dai and Q. Wang, *Biomaterials*, 2013, **34**, 3639–3646.

18 C. Sun, B. Li, M. Zhao, S. Wang, Z. Lei, L. Lu, H. Zhang, L. Feng, C. Dou, D. Yin, H. Xu, Y. Cheng and F. Zhang, *J. Am. Chem. Soc.*, 2019, **141**, 19221–19225.

19 Y. Li, Y. Liu, Q. Li, X. Zeng, T. Tian, W. Zhou, Y. Cui, X. Wang, X. Cheng, Q. Ding, X. Wang, J. Wu, H. Deng, Y. Li, X. Meng, Z. Deng, X. Hong and Y. Xiao, *Chem. Sci.*, 2020, **11**, 2621–2626.

20 L. Lu, B. Li, S. Ding, Y. Fan, S. Wang, C. Sun, M. Zhao, C. X. Zhao and F. Zhang, *Nat. Commun.*, 2020, **11**, 4192.

21 E. D. Cosco, I. Lim and E. M. Sletten, *ChemPhotoChem*, 2021, DOI: 10.1002/cptc.202100045.

22 H. Wan, J. Yue, S. Zhu, T. Uno, X. Zhang, Q. Yang, K. Yu, G. Hong, J. Wang, L. Li, Z. Ma, H. Gao, Y. Zhong, J. Su, A. L. Antaris, Y. Xia, J. Luo, Y. Liang and H. Dai, *Nat. Commun.*, 2018, **9**, 1171.

23 W. Wang, Z. Ma, S. Zhu, H. Wan, J. Yue, H. Ma, R. Ma, Q. Yang, Z. Wang, Q. Li, Y. Qian, C. Yue, Y. Wang, L. Fan,

Y. Zhong, Y. Zhou, H. Gao, J. Ruan, Z. Hu, Y. Liang and H. Dai, *Adv. Mater.*, 2018, **30**, 1800106.

24 M. Pengshung, J. Li, F. Mukadum, S. A. Lopez and E. M. Sletten, *Org. Lett.*, 2020, **22**, 6150–6154.

25 J. B. Grimm, A. K. Muthusamy, Y. Liang, T. A. Brown, W. C. Lemon, R. Patel, R. Lu, J. J. Macklin, P. J. Keller, N. Ji and L. D. Lavis, *Nat. Methods*, 2017, **14**, 987–994.

26 M. Li, S. Long, Y. Kang, L. Guo, J. Wang, J. Fan, J. Du and X. Peng, *J. Am. Chem. Soc.*, 2018, **140**, 15820–15826.

27 J. Bucevičius, G. Kostiuk, R. Gerasimaitė, T. Gilat and G. Lukinavičius, *Chem. Sci.*, 2020, **11**, 7313–7323.

28 L. D. Lavis, *Biochemistry*, 2017, **56**, 5165–5170.

29 M. Dai, Y. J. Reo, C. W. Song, Y. J. Yang and K. H. Ahn, *Chem. Sci.*, 2020, **11**, 8901–8911.

30 N. Y. Kang, J. Y. Lee, S. H. Lee, I. H. Song, Y. H. Hwang, M. J. Kim, W. H. Phue, B. K. Agrawalla, S. Y. D. Wan, J. Lalic, S. J. Park, J. J. Kim, H. Y. Kwon, S. H. Im, M. A. Bae, J. H. Ahn, C. S. Lim, A. K. K. Teo, S. Park, S. E. Kim, B. C. Lee, D. Y. Lee and Y. T. Chang, *J. Am. Chem. Soc.*, 2020, **142**, 3430–3439.

31 A. J. Huckaba, F. Giordano, L. E. McNamara, K. M. Dreux, N. I. Hammer, G. S. Tschumper, S. M. Zakeeruddin, M. Grätzel, M. K. Nazeeruddin and J. H. Delcamp, *Adv. Energy Mater.*, 2015, **5**, 1401629.

32 J. Gayton, S. A. Autry, W. Meador, S. R. Parkin, G. A. Hill, N. I. Hammer and J. H. Delcamp, *J. Org. Chem.*, 2019, **84**, 687–697.

33 W. E. Meador, S. A. Autry, R. N. Bessetti, J. N. Gayton, A. S. Flynt, N. I. Hammer and J. H. Delcamp, *J. Org. Chem.*, 2020, **85**, 4089–4095.

34 L. E. McNamara, T. A. Rill, A. J. Huckaba, V. Ganeshraj, J. Gayton, R. A. Nelson, E. A. Sharpe, A. Dass, N. I. Hammer and J. H. Delcamp, *Chem. –Eur. J.*, 2017, **23**, 12494–12501.

35 C. S. L. Rathnamalala, J. N. Gayton, A. L. Dorris, S. A. Autry, W. Meador, N. I. Hammer, J. H. Delcamp and C. N. Scott, *J. Org. Chem.*, 2019, **84**, 13186–13193.

36 E. W. Miller, A. E. Albers, A. Pralle, E. Y. Isacoff and C. J. Cheng, *J. Am. Chem. Soc.*, 2005, **127**, 16652–16659.

37 A. D. Becke, *J. Chem. Phys.*, 1993, **98**, 5648–5652.

38 C. Lee, W. Yang and R. G. Parr, *Phys. Rev. B*, 1988, **37**, 785–789.

39 M. J. Frisch, J. A. Pople and J. S. Binkley, *J. Chem. Phys.*, 1983, **80**, 3265–3269.

40 I. Chandrasiri, D. G. Abebe, M. Loku Yaddehige, J. S. D. Williams, M. F. Zia, A. Dorris, A. Barker, B. L. Simms, A. Parker, B. P. Vinjamuri, N. Le, J. N. Gayton, M. B. Chougule, N. I. Hammer, A. Flynt, J. H. Delcamp and D. L. Watkins, *ACS Appl. Bio Mater.*, 2020, **3**, 5664–5677.